

Chemical composition of halo and disk stars with overlapping metallicities^{*,**}

P.E. Nissen¹ and W.J. Schuster²

¹ Institute of Physics and Astronomy, University of Aarhus, DK-8000 Aarhus C, Denmark

² Observatorio Astronómico Nacional, UNAM, Apartado Postal 877, C.P. 22800 Ensenada, B.C., México

Received 7 February 1997 / Accepted 30 April 1997

Abstract. High resolution ($R = 60\,000$), high S/N spectra have been obtained for 13 halo stars and 16 disk stars with $5400 \lesssim T_{\text{eff}} \lesssim 6500$ K, $4.0 \lesssim \log g \lesssim 4.6$ and overlapping metallicities in the range $-1.3 \lesssim [\text{Fe}/\text{H}] \lesssim -0.5$. Equivalent widths of weak Fe I and Fe II lines are used to determine differential values of T_{eff} and $\log g$. Relative abundances of O, Na, Mg, Si, Ca, Ti, Cr, Fe, Ni, Y and Ba are determined to a precision ranging from 0.02 to 0.07 dex. Kinematical data have been collected and used to calculate the stellar orbital parameters, R_{max} , the maximum distance from the Galactic center, and z_{max} , the maximum distance from the Galactic plane.

A group of 8 halo stars have significantly lower $[\alpha/\text{Fe}]$ values than disk stars of the same metallicity ($\alpha \equiv \text{O, Mg, Si, Ca or Ti}$). These stars are also underabundant in Na and Ni and maybe in Cr. $[\text{Na}/\text{Fe}]$ ranges from -0.4 to $+0.1$, and $[\text{Ni}/\text{Fe}]$ is surprisingly well correlated with $[\text{Na}/\text{Fe}]$. The smallest values of $[\alpha/\text{Fe}]$ and $[\text{Na}/\text{Fe}]$ are found for the stars with the largest values of R_{max} and z_{max} . This may indicate that the anomalous halo stars have been accreted from dwarf galaxies with a chemical evolution history different from that of the inner halo and the disk. In any case the data show that abundance ratios in stars are not universal functions of $[\text{Fe}/\text{H}]$ and that the chemical evolution of the Galaxy at $[\text{Fe}/\text{H}] \simeq -1.0$ is more complicated than assumed in many models.

One halo star, HD 106038, is found to be strongly overabundant in Si, Ni, Y and Ba relative to Fe.

Key words: stars: abundances; Population II – Galaxy: abundances – Galaxy: evolution – Galaxy: halo

Send offprint requests to: P.E. Nissen

* Tables A1-A5 are only available in electronic form at CDS via anonymous ftp to cdsarc.u-strasbg.fr (130.79.128.5) or via <http://cdsweb.u-strasbg.fr/Abstract.html>

** Based on observations carried out at the European Southern Observatory, La Silla, Chile

1. Introduction

Recent surveys of high-velocity stars in the solar neighborhood have revealed an interesting distribution of the stars in a diagram where the stellar velocity component in the direction of the Galactic rotation, V_{rot} , is plotted as a function of the metallicity, $[\text{Fe}/\text{H}]$. Fig. 5 of Schuster et al. (1993) shows such a diagram for 1149 high-velocity stars with $[\text{Fe}/\text{H}]$ and distances determined from Strömberg $uvby-\beta$ photometry, and Fig. 1 of Carney et al. (1996) shows a similar diagram for 1022 high proper motion stars, for which the metallicities and the radial velocities were determined from low-S/N, high-resolution echelle spectra. In both diagrams it is striking that the metallicity range $-1.3 \lesssim [\text{Fe}/\text{H}] \lesssim -0.5$ contains both fast rotating (thick-disk) stars and slow rotating (halo) stars with a fairly clear separation between the two groups. The distribution of stars does not support a smooth transition from slow rotating metal-poor halo stars to fast rotating metal-rich disk stars, as expected from the classical ELS model (Eggen et al. 1962). Instead, the $V_{\text{rot}}, [\text{Fe}/\text{H}]$ diagrams point to the existence of two distinct populations with a considerable degree of overlap in metallicity. This interpretation is supported by the extensive statistical study of Beers & Sommer-Larsen (1995) of nearly 2000 Galactic stars selected without kinematic bias. In the metallicity interval $-1.5 \lesssim [\text{Fe}/\text{H}] \lesssim -1.0$ the fraction of thick-disk stars in the solar neighborhood appears to be as high as 60%. For $[\text{Fe}/\text{H}] > -1.0$ the large majority of stars belong to either the thick-disk or the thin-disk populations, but slow rotating stars do exist.

As discussed by Norris (1996) the kinematics and metallicities of stars representing the halo-disk transition are of high interest in connection with studies of the formation and evolution of the Galaxy. Overall metallicity is, however, only one of the chemical parameters that provide information on Galactic evolution. Abundance ratios between some elements, e.g. O/Fe or Mg/Fe, depend on the IMF and/or the timescale for the chemical evolution (Wyse & Gilmore 1993, Pagel & Tautvaišienė 1995, Matteucci 1996). Therefore, in the present paper a detailed study of the chemical composition of halo and disk stars with overlapping metallicities is presented. The study aims

at a very high internal precision of the abundances, so that even small differences in the chemical composition can be revealed.

2. Selection of stars

The program stars were selected from the catalogues of *wby*- β photometry of high-velocity stars by Schuster & Nissen (1988) and Schuster et al. (1993). Using the calibrations by Schuster & Nissen (1989) and Nissen & Schuster (1991) main sequence stars and subgiants with $0.25 < (b - y)_0 < 0.45$ and $-1.3 \lesssim [\text{Fe}/\text{H}] \lesssim -0.5$ were first picked out. Among these stars two groups were defined according to the criteria:

- i) $V_{\text{rot}} < 50 \text{ km s}^{-1}$; the *halo* stars.
- ii) $V_{\text{rot}} > 150 \text{ km s}^{-1}$; the *disk* stars.

We aimed at observing about the same number of halo and disk stars, and furthermore to have as far as possible the same distribution in $[\text{Fe}/\text{H}]$ for the two groups.

Obviously, one cannot be sure that each individual star has been classified correctly as halo or disk, but the probability of correct classification seems high. The mean velocity of Galactic thick-disk stars is $\langle V_{\text{rot}} \rangle \simeq 200 \text{ km s}^{-1}$ and the dispersion is of the order of $\pm 40 \text{ km s}^{-1}$ (Beers & Sommer-Larsen 1995). Stars with $V_{\text{rot}} < 50 \text{ km s}^{-1}$ therefore have a very high probability of being genuine halo stars. Halo stars have $\langle V_{\text{rot}} \rangle \simeq 0 \text{ km s}^{-1}$ with a dispersion of $\pm 90 \text{ km s}^{-1}$; so some of the stars with $V_{\text{rot}} > 150 \text{ km s}^{-1}$ could be halo stars. If, however, the ratio of the number of thick-disk stars to the number of halo stars is greater than one for $[\text{Fe}/\text{H}] \gtrsim -1.3$, as suggested by the work of Beers & Sommer-Larsen (1995), then it is highly probable that stars with $V_{\text{rot}} > 150 \text{ km s}^{-1}$ are indeed disk stars.

Among the group of disk stars no attempt has been made to distinguish between thick-disk and thin-disk stars, because the difference of the mean Galactic rotational velocity of the two groups is of the same order as the velocity dispersion for the thick-disk stars, $\sigma(V_{\text{rot}}) \simeq 40 \text{ km s}^{-1}$. In the following these stars will just be referred to as *disk* stars. It is noted, however, that the average asymmetric Strömberg drift of our disk stars is $-46.0 \pm 26.7 \text{ km s}^{-1}$ indicating a really old component of the disk (Mihalas & Binney 1981).

In Table 1 all stars observed are listed together with quantities derived from the *wby*- β photometry. The color excesses and the metallicities have been calculated according to the calibrations of Schuster & Nissen (1989). If $E(b - y) > 0.015$ the star is assumed to be reddened and the photometric indices have been corrected accordingly. If β is not available or $\beta < 2.55$, the color excess could not be calculated and $E(b - y) = 0.0$ is assumed. One of the stars, HD 76932 = HR 3578, classified as a disk star, has V_{rot} slightly below the limit of 150 km s^{-1} . It was included as one of the bright, metal-poor stars from the large survey of the chemical composition of disk stars by Edvardsson et al. (1993) and will be used as a standard star (together with HD 22879) in the differential abundance analysis of the whole sample.

Tables with detailed information about photometry and kinematics are available in electronic form; see Appendix.

Table 1. List of program stars including the intrinsic color index $(b - y)_0$, the color excess $E(b - y)$, and the photometric metallicity $[\text{Fe}/\text{H}]$ as well as the Galactic rotational velocity of the star and its corresponding classification as halo (H) or disk (D) star

Star	$(b - y)_0$	$E(b - y)$	$[\text{Fe}/\text{H}]$	V_{rot} km/s	
HD3567	0.332	-0.002	-1.18	18	H
-61 0282	0.365	-0.012	-1.10	-19	H
HD17288	0.378	-0.016	-0.74	151	D
HD17820	0.377	0.002	-0.76	154	D
G005-040	0.376	0.026	-0.81	32	H
-47 1087	0.387	-0.009	-0.85	178	D
HD22879	0.370	-0.004	-0.87	158	D
HD24339	0.369	-0.016	-0.74	180	D
HD25704	0.371	-0.015	-0.84	176	D
HD241253	0.357	-0.007	-0.91	178	D
G102-020	0.435		-1.29	168	D
-33 3337	0.334		-1.21	190	D
-57 1633	0.343		-0.81	-7	H
-45 3283	0.384		-0.92	-10	H
G088-040	0.351	-0.006	-0.85	162	D
HD76932	0.354	-0.025	-0.80	145	D
G046-031	0.350	-0.016	-0.73	-42	H
HD83220	0.285	0.005	-0.72	248	D
-21 3420	0.354	-0.021	-0.97	151	D
HD103723	0.329	0.027	-0.91	42	H
HD105004	0.360	0.027	-0.74	-13	H
HD106038	0.342	-0.018	-1.09	-2	H
HD106516	0.318	-0.017	-0.82	175	D
W7547	0.337	0.012	-0.64	31	H
HD113083	0.376	0.011	-0.93	19	H
HD113679	0.404		-0.93	-69	H
HD120559	0.424	0.005	-0.92	183	D
HD121004	0.395	0.012	-0.83	-34	H
HD126681	0.400	-0.013	-1.16	195	D

3. Observations and data reduction

The observations were carried out with the ESO NTT 3.5m telescope during 4 clear nights, January 2-6, 1996. The EMMI spectrograph was used in the high resolution echelle mode. Instead of the standard R2 echelle grating, a new R4 grating (blaze angle = 76°) was employed (Dekker et al. 1994). This doubled the spectral resolution to about 60 000 for an entrance slit of $1''$. As the seeing was better than this most of the time, the throughput at the slit was quite high.

A thinned 2048×2048 SITe CCD detector with a quantum efficiency of about 60% in the 4000 - 8000 Å region was employed. This spectral region was covered by the CCD for the grism cross disperser chosen, but since the echelle orders are very closely packed in the bluest part, only orders with $\lambda > 5000\text{Å}$ were extracted. Furthermore, some of the reddest spectral orders are overlapped by blue orders from the 2^{nd} -order grism spectrum and could not be used.

Standard IRAF tasks were used for bias subtraction, flat-fielding, correction for scattered light as estimated between the

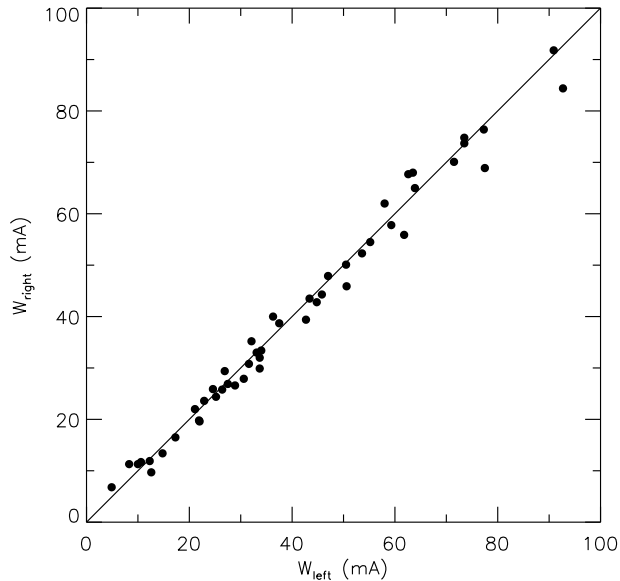


Fig. 1. A comparison of two sets of equivalent widths measured in the left and the right part of consecutive echelle orders in the spectrum of CD-45 3283

spectral orders, extraction of 51 echelle orders, wavelength calibration by the aid of a thorium spectrum, and fitting of a continuum to each order. Equivalent widths were then measured by fitting Gaussians to the lines. Since only rather weak lines were included, this gives a higher accuracy than area integration, which is more affected by blends in the outer parts of the lines.

Altogether 13 halo stars and 16 disk stars were observed. Most of them have magnitudes between $m_V = 9$ and 11. The S/N of the spectra ranges from about 180 in the central part of the echelle orders to about 140 at the edges of the orders. A typical integration time for a $m_V = 10$ magnitude star was 1 hour. Fainter stars were observed several times and the spectra coadded so that cosmic ray disturbances could be effectively removed.

From 5000 to 6000 Å there is considerable overlap in wavelength between two consecutive echelle orders. The equivalent widths of many lines could therefore be measured twice and used to estimate the precision. Fig. 1 shows a typical example for one of the fainter program stars, CD-45 3283, $m_V = 10.6$. As seen the agreement between the two sets of equivalent widths is very satisfactory; the rms dispersion around the 1:1 line is 1.5 mÅ corresponding to a precision of about 1 mÅ for a single measurement.

Table 2 lists the number of lines measured for various elements; in some cases lines from two ionization stages are available. For the most metal-poor stars the weakest lines could not be measured and the number of lines is somewhat smaller. A detailed list of the lines and the equivalent widths measured is available in electronic form; see Appendix.

Table 2. List of elements and the number, N , of neutral and ionized lines, for which the equivalent width was measured. For elements with fewer than 6 lines the wavelengths of these are given

	N	Wavelength (Å)
O I	3	7772.0, 7774.2, 7775.4
Na I	4	5682.7, 5688.2, 6154.2, 6160.8
Mg I	1	5711.1
Si I	15	
Si II	1	6347.1
Ca I	17	
Ti I	7	
Ti II	3	5185.9, 5336.8, 5381.0
Cr I	7	
Cr II	5	5237.3, 5305.9, 5308.4, 5313.6, 5334.9
Fe I	104	
Fe II	12	
Ni I	23	
Y II	4	5087.4, 5123.2, 5200.4, 5509.9
Ba II	3	5853.7, 6141.7, 6496.9

4. Stellar parameters and chemical abundances

4.1. Model atmospheres and line calculations

The abundance analysis of the measured equivalent widths is based on a net of flux constant, homogeneous, LTE model atmospheres kindly supplied by Bengt Edvardsson, Uppsala. The models were computed with an updated version of the MARCS code of Gustafsson et al. (1975) using continuous opacities from Asplund et al. (1997) and including UV line blanketing as described by Edvardsson et al. (1993). Convection was treated in the mixing-length approximation of Henyey et al. (1965) with $\ell/H_p = 1.5$ and $y = 0.076$. Abundance ratios in the models with respect to iron are assumed to be solar, but it was checked that the assumption of enhanced α -element abundances ($\alpha \equiv \text{O, Ne, Mg, Si, S, Ca, and Ti}$) with $[\alpha/\text{Fe}] = +0.3$ dex has negligible effects on the differential abundance ratios derived.

A program, EQWIDTH, kindly made available from the Uppsala stellar atmospheric group, was used to calculate equivalent widths for the models and to interpolate to the abundances that match the observed and calculated equivalent widths. In addition to thermal and microturbulent Doppler broadening of the lines, van der Waals damping was also included. Correction factors to the classical van der Waals damping widths were taken from Edvardsson et al. (1993). As only lines weaker than about 90 mÅ were included in the abundance analysis, the values of these correction factors are not critical.

The calculation of the equivalent widths is based on the assumption of LTE. Deviations from LTE may well occur for some of the lines, e.g. the oxygen triplet at 7774 Å, but since the stars are limited to rather narrow intervals in effective temperature, gravity and metallicity, the effects on the differential abundances are probably small. For the same reason it is expected that errors in the models, due to the neglect of inhomogeneities and the handling of convection in the mixing-length approximation,

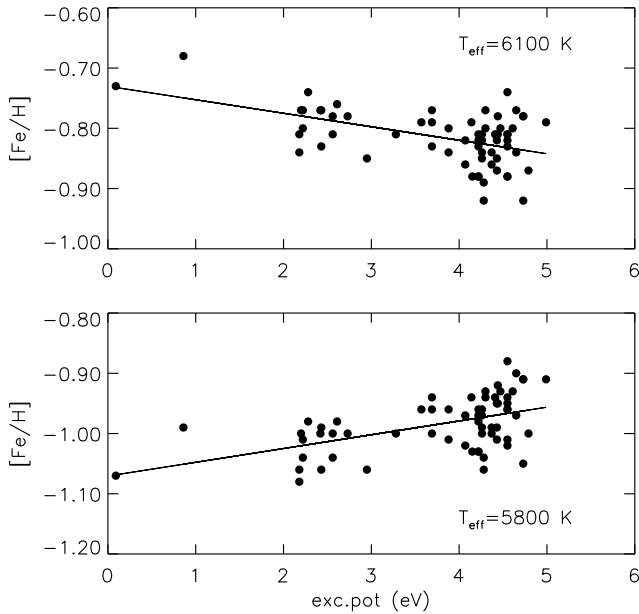


Fig. 2. $[\text{Fe}/\text{H}]$ of CD-57 1633 as derived from Fe I lines plotted vs. excitation potential of the lower energy level of the line. The two figures correspond to atmospheric models with different effective temperatures. In both cases the models have $\log g = 4.1$ and $[\text{Fe}/\text{H}] = -0.8$

have only limited effects on the derived differential abundances of halo and disk stars.

The gf -values of the lines were derived from an “inverted” abundance analysis of two bright stars, HD 22879 and HD 76932, which are included in the accurate study of disk stars by Edvardsson et al. (1993). Both were observed at the ESO NTT with a particularly high S/N of about 250. For these stars the values of the atmospheric parameters T_{eff} , $\log g$, and $[\text{Fe}/\text{H}]$ were taken from Edvardsson et al., and the following abundance ratios with respect to iron were assumed: $[\text{O}/\text{Fe}] = [\text{Mg}/\text{Fe}] = 0.3$, $[\text{Si}/\text{Fe}] = [\text{Ca}/\text{Fe}] = [\text{Ti}/\text{Fe}] = 0.2$, and $[\text{Na}/\text{Fe}] = 0.1$. For the rest of the elements solar ratios were adopted. These abundance ratios reflect the results of Edvardsson et al. (1993) for abundance ratios of disk stars with $[\text{Fe}/\text{H}] \simeq -0.8$; see their Fig. 15. The two gf -values of a given line determined for HD 22879 and HD 76932, respectively, agree in most cases within 0.05 dex and consequently the mean value was adopted as the final gf .

4.2. Stellar atmospheric parameters

Effective temperatures are determined from the excitation balance of Fe I lines. As an example, Fig. 2 shows the derived Fe abundances of CD-57 1633 versus excitation potential, χ , of the lower energy level of the line for two model atmospheres with $T_{\text{eff}} = 5800$ and 6100 K, respectively. Both models have $\log g = 4.1$, and $[\text{Fe}/\text{H}] = -0.80$. The figure includes only lines with $\log(W/\lambda) < -5.15$, i.e. lines with equivalent widths less than about 40 mÅ, in order to avoid lines that are sensitive to the adopted value of the microturbulent velocity. For $T_{\text{eff}} = 6100$ K

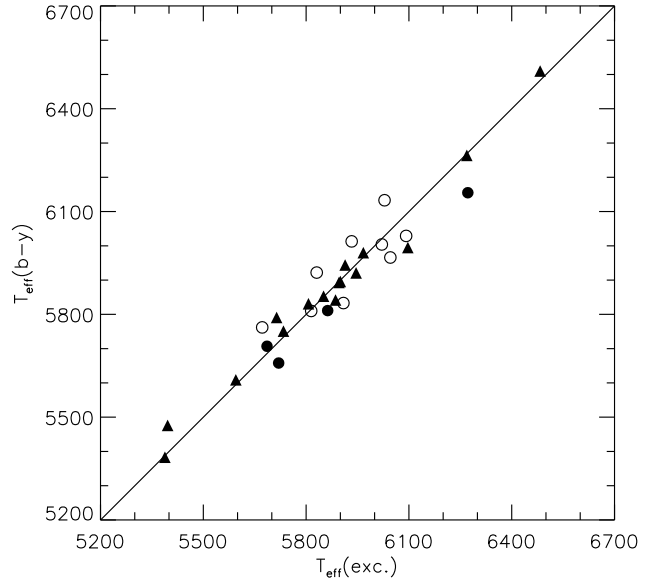


Fig. 3. A comparison of effective temperatures determined from the excitation balance of Fe I lines, and from $(b - y)_0$ using the model atmosphere calibration of Edvardsson et al. (1993). Disk stars are shown with filled triangles and halo stars with filled and open circles subdivided as described in Sect. 6

the slope of the straight line fit is $b = -0.022 \pm 0.006$, whereas $T_{\text{eff}} = 5800$ K gives $b = 0.023 \pm 0.006$. In both cases $\sigma([\text{Fe}/\text{H}]) \simeq 0.04$ dex. From this we find the effective temperature of CD-57 1633 to be close to 5950 K.

Using a similar technique the microturbulent velocity, ξ , can be determined from the slope of $[\text{Fe}/\text{H}]$ vs. equivalent width. Here, only lines with $\chi > 4$ eV were included in order to decouple the microturbulence determination from the T_{eff} determination. The precision of the determination is $\sigma(\xi) = 0.15 \text{ km s}^{-1}$. Within this error our microturbulent velocities are well fitted by the relation found by Edvardsson et al. (1993)

$$\xi = 1.25 + 8 \cdot 10^{-4} (T_{\text{eff}} - 6000) - 1.3 (\log g - 4.5) \text{ km s}^{-1} \quad (1)$$

except for one star, HD 113083, a spectroscopic binary, for which both components have a microturbulent velocity 0.6 km s^{-1} higher than the value corresponding to Eq. (1).

Having determined T_{eff} and $[\text{Fe}/\text{H}]$ from neutral iron lines, the gravity is determined by requiring that the iron abundance determined from Fe I and Fe II lines should be the same. As there are available more than 10 Fe II lines, this method gives $\log g$ with a high internal precision, provided that the degree of non-LTE over-ionization is not a strongly varying function of the stellar parameters.

The whole procedure of determining T_{eff} , $\log g$, $[\text{Fe}/\text{H}]$ and ξ has to be iterated to consistency, because the slope coefficient of $[\text{Fe}/\text{H}]$ vs. χ depends slightly on $\log g$, and the determination of gravity from the Fe I/Fe II balance depends on $[\text{Fe}/\text{H}]$.

Table 3 gives the final model atmosphere parameters of the stars. The precision of the parameters are: $\sigma(T_{\text{eff}}) = 50$ K, $\sigma(\log g) = 0.1$ dex, and $\sigma([\text{Fe}/\text{H}]) = 0.05$. We emphasize that

Table 3. Atmospheric parameters and chemical abundances of the program stars, classified as halo (H) or disk (D). Halo stars that are deficient in Na and Ni relative to Fe and less over-abundant in the α -elements than the disk stars are marked with an open circle. This table is also available in electronic form; see Appendix

Star	T_{eff}	$\log g$	[Fe/H]	$[\frac{\text{O}}{\text{Fe}}]$	$[\frac{\text{Mg}}{\text{Fe}}]$	$[\frac{\text{Si}}{\text{Fe}}]$	$[\frac{\text{Ca}}{\text{Fe}}]$	$[\frac{\text{Ti}}{\text{Fe}}]$	$[\frac{\text{Cr}}{\text{Fe}}]$	$[\frac{\text{Ni}}{\text{Fe}}]$	$[\frac{\text{Na}}{\text{Fe}}]$	$[\frac{\text{Y}}{\text{Fe}}]$	$[\frac{\text{Ba}}{\text{Fe}}]$		
HD3567	H	6092	4.08	-1.18	.20	.16	.12	.22	.16	-.01	-.11	-.25	-.07	.02	○
-61 0282	H	5909	4.46	-1.15	.14	.18	.14	.18	.15	-.04	-.10	-.24	-.17	-.06	○
HD17288	D	5714	4.44	-.88	.28	.24	.17	.17	.16	-.03	.01	.08	-.06	-.05	
HD17820	D	5807	4.24	-.67	.25	.25	.19	.19	.20	.03	.03	.17	-.08	-.17	
G005-040	H	5863	4.24	-.83	.31	.28	.24	.22	.20	.01	.02	.16	.04	.01	
-47 1087	D	5734	4.38	-.76	.28	.26	.19	.17	.17	-.02	-.01	.08	-.02	-.06	
HD22879	D	5851	4.36	-.82	.30	.29	.20	.19	.19	.00	-.01	.09	-.02	-.01	
HD24339	D	5900	4.37	-.63	.23	.20	.16	.14	.23	.01	.02	.15	-.11	-.08	
HD25704	D	5886	4.33	-.85	.23	.24	.14	.16	.15	.01	-.01	.14	-.16	-.08	
HD241253	D	5896	4.36	-1.07	.33	.30	.24	.19	.16	-.04	-.03	.05	-.01	.06	
G102-020	D	5388	4.62	-1.08	.23	.21	.12	.14	.21	-.01	-.06	.01	-.03	-.13	
-33 3337	D	6097	4.09	-1.30	.29	.36	.18	.20	.28	.00	.02	.15	-.01	-.01	
-57 1633	H	5933	4.26	-.90	.05	.03	.00	.09	.02	-.05	-.16	-.26	-.27	-.10	○
-45 3283	H	5672	4.57	-.83	.05	.04	.00	.05	.02	-.06	-.18	-.34	-.17	-.04	○
G088-040	D	5967	4.26	-.80	.21	.24	.14	.12	.17	-.01	.01	.15	-.14	-.04	
HD76932	D	5914	4.23	-.85	.30	.30	.20	.20	.21	.00	.00	.11	.00	.01	
G046-031	H	6021	4.44	-.75	.10	.07	.01	.08	.08	-.01	-.13	-.10	-.03	.04	○
HD83220	D	6483	4.22	-.47	.09	.05	.02	.04	.00	-.02	-.02	.14	-.03	.01	
-21 3420	D	5946	4.41	-1.04	.30	.28	.25	.22	.21	-.01	.01	-.04	-.01	.12	
HD103723	H	6029	4.32	-.79	.09	.03	.02	.13	.09	-.02	-.11	-.14	-.12	-.01	○
HD105004	H	5831	4.36	-.80	.05	.11	.04	.06	.01	-.05	-.07	-.04	-.19	-.09	○
HD106038	H	6046	4.46	-1.26	.30	.36	.57	.21	.19	.02	.18	.14	.39	.49	
HD106516	D	6269	4.51	-.61	.25	.29	.19	.17	.18	.02	.00	.09	-.07	-.03	
W7547	H	6272	4.03	-.42	.05	.04	.08	.09	.03	.05	-.01	.16	-.04	.09	
HD113083A	H	5865	4.41	-.93	.02	.14	.10	.11	.08	-.04	-.06	.03	-.05	-.09	○
HD113083B	H	5764	4.38	-.91	.12	.14	.12	.11	.07	-.07	-.08	-.04	-.01	-.09	○
HD113679	H	5720	4.14	-.65	.32	.23	.23	.21	.20	.01	.02	.12	-.02	-.10	
HD120559	D	5396	4.38	-.93	.39	.30	.19	.16	.20	-.02	-.01	.10	-.07	-.22	
HD121004	H	5686	4.40	-.70	.25	.26	.20	.19	.20	.01	-.01	.14	.04	-.08	
HD126681	D	5595	4.43	-1.12	.22	.31	.27	.24	.21	-.01	-.05	-.03	.14	.13	

these are internal errors for the parameters relative to the adopted parameters of HD 22879 and HD 76932.

In order to check the precision of the effective temperatures, $T_{\text{eff}}(\text{exc.})$ has been compared with $T_{\text{eff}}(b-y)$, the effective temperature derived from $(b-y)_0$ using the model atmosphere calibration of Edvardsson et al. (1993). As seen in Fig. 3 there is an excellent agreement between the two ways of determining T_{eff} . The rms scatter around the 1:1 line is 57 K, which is what one would expect if the error of both sets of T_{eff} is 40 K. Still, it is preferable to use $T_{\text{eff}}(\text{exc.})$ in our abundance analysis because in some cases the color index could be significantly disturbed by a small amount of undetected reddening or by the presence of a faint red binary component.

HD 113083 is a double-lined binary with nearly identical sets of lines. According to Lindgren et al. (1989) the orbital period is 23.82 days, and the two components have practically the same mass. The analysis of each component's spectrum leads to a small difference in T_{eff} of about 100 K. Assuming that the two stars lie on a 16 Gyr isochrone in the $M_V - T_{\text{eff}}$ plane, the corresponding luminosity ratio is $\simeq 1.2$ (Bergbusch & Vandenberg 1992). This ratio was adopted when correcting the measured

equivalent widths of one component for the contribution to the continuum light from the other component. As seen in Table 3 the abundances of the two components agree very well.

According to Lindgren (1994), HD 83220 and HD 106516 are SB1's, and Carney et al. (1994) list G102-020 and G046-031 as single-lined binaries with preliminary orbits. Our high resolution spectra show no sign of a secondary spectrum for any of these stars; so it is assumed that the effect of the secondary on the primary spectrum is negligible.

4.3. Abundance ratios and their errors

The derived abundance ratios with respect to iron are given in Table 3. Following T_{eff} , $\log g$ and the iron-to-hydrogen ratio, first the α -elements O, Mg, Si, Ca and Ti are listed, then the iron peak elements Cr and Ni, then Na, and finally the s -process elements Y and Ba.

The "standard" stars, HD 22879 and HD 76932, were analyzed in the same way as the other stars. As expected, T_{eff} , $\log g$, and [Fe/H] agree closely with the values of Edvardsson et al.

Table 4. Estimated internal errors of various abundance ratios. Column 2 gives the error due to the uncertainty of the equivalent width measurements; N being the number of lines used (see Table 2). Column 3-5 give the changes of the abundance ratios corresponding to the listed changes in the model atmosphere parameters. Errors due to the uncertainty of $[\text{Fe}/\text{H}]$ of the model are negligible. The last column gives the total error assuming that the individual errors are uncorrelated

	$\frac{0.05}{\sqrt{N}}$	ΔT_{eff} +50 K	$\Delta \log g$ +0.10	$\Delta(\xi)$ +0.15 km/s	σ_{tot}
$\sigma[\text{Fe}/\text{H}]$.005	+.029	+.009	-.017	.035
$\sigma[\text{O}/\text{Fe}]$.028	-.067	+.021	+.007	.076
$\sigma[\text{Na}/\text{Fe}]$.025	-.009	-.010	+.012	.031
$\sigma[\text{Mg}/\text{Fe}]$.050	-.007	-.013	+.007	.053
$\sigma[\text{Si}/\text{Fe}]$.014	-.016	-.002	+.016	.027
$\sigma[\text{Ca}/\text{Fe}]$.013	-.003	-.008	+.004	.016
$\sigma[\text{Ti}/\text{Fe}]$.020	+.014	-.005	+.012	.028
$\sigma[\text{Cr}/\text{Fe}]$.020	+.009	-.003	+.001	.022
$\sigma[\text{Ni}/\text{Fe}]$.012	+.003	-.003	+.011	.017
$\sigma[\text{Y}/\text{Fe}]$.025	-.014	+.034	+.011	.046
$\sigma[\text{Ba}/\text{Fe}]$.028	-.015	+.044	-.023	.059
$\sigma[\text{Si}_{\text{SiI}}/\text{Si}_{\text{SiII}}]$.050	+.050	-.035	-.001	.079
$\sigma[\text{Ti}_{\text{TiI}}/\text{Ti}_{\text{TiII}}]$.034	+.037	-.047	-.008	.069
$\sigma[\text{Cr}_{\text{CrI}}/\text{Cr}_{\text{CrII}}]$.030	+.043	-.036	-.010	.064

(1993), and the abundance ratios agree within ± 0.01 with those adopted in Sect. 4.1, when determining the gf -values.

Since the aim of the study is to search for small abundance differences between disk and halo stars, a careful evaluation of errors is needed. As will be seen from the following discussion very small errors are claimed for some of the abundance ratios. These errors are valid for abundance differences within the present sample of stars. Relative to other stars, including the Sun, the errors are larger.

A significant error source is the equivalent width measurements. In Sect. 3 the error in W was estimated to be ± 1 mÅ from a comparison of lines measured in consecutive echelle orders, but this does not include possible effects of blends or systematic errors in the continuum setting. An error of 2 to 3 mÅ in W is probably more realistic. For a typical line having an equivalent width of 20 to 30 mÅ the corresponding error of the abundance is of the order of 0.05 dex. An independent estimate comes from the rms scatter of $[\text{Fe}/\text{H}]$ determined from the individual Fe I lines. The average scatter for the sample of stars (excluding HD 22879 and HD 76932) is $\langle \sigma[\text{Fe}/\text{H}] \rangle = 0.05$. A similar value is obtained for other elements with many lines, i.e. Si, Ca and Ni. Hence, the equivalent width error can be assumed to correspond to an abundance error of $\pm 0.05/\sqrt{N}$, where N is the number of lines measured.

The other major error source is the uncertainty of the stellar atmospheric parameters. It can be estimated by perturbing these parameters with amounts corresponding to the typical errors given in Sect. 4.2. The result of this exercise is given in Table 4.

As seen from Table 4 the total error of $[\text{Ca}/\text{Fe}]$, $[\text{Cr}/\text{Fe}]$ and $[\text{Ni}/\text{Fe}]$ is as small as ± 0.02 dex. The abundances of these elements are based on many neutral lines, and the Ca, Cr and Ni

lines change in the same way as the Fe lines, when the atmospheric parameters are changed. The errors of $[\text{Na}/\text{Fe}]$, $[\text{Si}/\text{Fe}]$ and $[\text{Ti}/\text{Fe}]$ are also small (± 0.03), whereas the error of $[\text{Mg}/\text{Fe}]$ is ± 0.05 , because only one line was measured. A similar error is expected for Y and Ba; their abundances are based on ionized lines and hence fairly sensitive to errors in the gravity parameter. Finally, the error in $[\text{O}/\text{Fe}]$ is relatively large because the oxygen triplet lines and the Fe I lines depend in the opposite way on T_{eff} .

In the case of Si, Ti and Cr both neutral and ionized lines have been used to determine the abundances. The following average differences and dispersions for the sample of stars are found:

$$\langle [\text{Si}_{\text{SiI}}/\text{Si}_{\text{SiII}}] \rangle = -0.004 \pm 0.071,$$

$$\langle [\text{Ti}_{\text{TiI}}/\text{Ti}_{\text{TiII}}] \rangle = +0.021 \pm 0.043,$$

$$\langle [\text{Cr}_{\text{CrI}}/\text{Cr}_{\text{CrII}}] \rangle = -0.024 \pm 0.067.$$

These measured dispersions are of the same order of size or, in the case of Ti, even smaller than the estimated errors in Table 4.

5. Kinematics and orbits of the stars

5.1. Kinematic data

As one of the aims of the present study is to search for possible correlations between abundance ratios and stellar orbital parameters, an effort has been made to obtain accurate values for the Galactic velocity components of the stars with respect to the LSR, U' , V' , and W' . The *wby* - β data referenced in Sect. 2 was used to determine photometric distances using the calibrations of Nissen & Schuster (1991). These distances include an evolutionary correction of the form, $\delta M_V = f \delta c_0$, where the f coefficient is taken from Nissen et al. (1987), and δc_0 is the displacement of a star in the $c_0, (b-y)_0$ diagram from its corresponding ZAMS. In the present calculations for distances the spectroscopic $[\text{Fe}/\text{H}]$ values have been substituted for the photometric values.

The proper motions used to calculate the Galactic velocities and initial conditions for the orbital integrations were taken in large part from the Hipparcos Input Catalogue (Turon et al. 1992). The only exception is the star G005-040, whose proper motion was taken from Fouts & Sandage (1986), based on the Lowell and Luyten proper motion surveys.

The radial velocities were selected from several sources according to their estimated observational errors; external comparisons, with the values of Carney et al. (1994) for example, indicate that our NTT values are accurate to $\sim \pm 3$ km s $^{-1}$. The principal sources for the radial velocities were Carney et al. (1994), Turon et al. (1992), and the NTT observations reported here. Several of these stars are spectroscopic binaries; the systematic radial velocity for HD83220 was taken from Lindgren (1994), that of HD106516 from Latham et al. (1992), and that for HD113083 from Lindgren et al. (1989). The halo star -57 1633 also shows evidence for a variable radial velocity; the final velocity used here is an average of our NTT value with three values taken from Barbier-Brossat & Petit (1986).

Table 5. Galactic velocity components with respect to the LSR and the computed orbital parameters. The stars are arranged in two groups; first the disk stars and then the halo stars

Star	U' km/s	V' km/s	W' km/s	R_{\max} kpc	R_{\min} kpc	z_{\max} kpc
HD17288	64	-76	57	9.2	4.1	1.1
HD17820	-38	-64	-56	8.8	4.8	1.0
-47 1087	70	-42	44	9.6	5.4	0.8
HD22879	98	-65	-41	10.2	4.3	0.7
HD24339	134	-43	23	12.2	4.7	0.4
HD25704	91	-41	-8	10.3	5.1	0.1
HD241253	-21	-50	74	8.7	5.8	1.6
G102-020	9	-48	65	8.6	5.8	1.2
-33 3337	-12	-34	-114	8.8	7.6	3.0
G088-040	-61	-57	-43	9.3	4.8	0.7
HD76932	39	-79	70	8.8	4.2	1.5
HD83220	-13	37	22	12.0	8.4	0.3
-21 3420	20	-65	-69	8.6	4.9	1.4
HD106516	-55	-47	-44	9.2	5.3	0.7
HD120559	26	-39	-36	8.7	5.9	0.5
HD126681	9	-24	-69	8.5	7.2	1.3
HD3567	-144	-203	-28	10.6	0.3	7.3
-61 0282	-260	-247	-33	17.6	0.4	10.2
G005-040	-137	-193	-68	10.9	0.4	6.3
-57 1633	229	-231	-41	14.9	0.1	12.2
-45 3283	251	-244	-72	17.4	0.6	8.5
G046-031	0	-270	79	9.0	1.0	4.0
HD103723	52	-175	70	9.1	0.8	4.5
HD105004	25	-187	-33	8.5	0.6	4.7
HD106038	-16	-236	36	8.5	0.2	5.7
W7547	463	-174	59	113.7	0.8	32.7
HD113083	-41	-221	106	9.5	0.1	7.3
HD113679	74	-263	1	9.0	0.7	0.1
HD121004	-66	-245	106	9.0	0.5	6.2

5.2. Orbit calculations

The numerical integration of the Galactic orbits was very kindly done for us by Christine Allen making use of the Galactic mass model of Allen & Santillán (1991). The details of these orbital integrations are very similar to those of Schuster & Allen (1997); the main difference here being that each orbit was integrated backwards in time for 2000 time steps or 16 Gyr, whichever came first, rather than 1000 time steps.

The Galactic mass model of Allen & Santillán (1991) consists of three components, a central spherical mass distribution and a disk, both of the Miyamoto-Nagai type, plus a massive spherical halo. It represents well the global Galactic characteristics which most determine an orbit, such as the rotation curve of the Galaxy and the vertical run of the perpendicular force. However, this model does not include a non-axisymmetric component; there is increasing evidence that the Milky Way may be a barred spiral (Blitz & Teuben 1996, chapter 2).

The simple, analytical form of this model's potential allows rapid, precise, and reproducible numerical orbit integrations. The present orbits were computed making use of a 7th-order

Runge-Kutta-Fehlberg integrator with automatic step-size control. (See Allen & Martos 1986; Allen & Santillán 1991). At the end of most orbital calculations the total energy and the Z -component of the angular momentum were conserved to better than $\Delta E/E < 10^{-6}$ and $\Delta h/h < 10^{-7}$, respectively. The output of the model provides orbital parameters such as R_{\max} , the maximum distance from the Galactic center attained by a star in its orbit; R_{\min} , the minimum distance; and z_{\max} , the maximum distance from the Galactic plane. In Table 5 are given these orbital parameters for the program stars plus the Galactic space velocities with respect to the Local Standard of Rest. Further orbital parameters such as the eccentricity and the z -component of the angular momentum are available in electronic form; see Appendix.

The calculations of the Galactic space velocities and their errors are based on the precepts and equations of Johnson & Soderblom (1987). In Allen et al. (1991) the propagation of the distance and velocity errors into the orbital parameters was investigated by calculating two additional orbits for each of a number of typical and interesting stars: one orbit from adding the estimated observational errors to the distances, proper motions, and radial velocities, and another orbit, subtracting these errors. Typical errors in z_{\max} fall in the range 20-30%. For R_{\max} the errors are generally somewhat smaller, 5-20%, except for stars that are weakly bound to the Galaxy, $R_{\max} \gtrsim 50$ kpc, where the errors in both R_{\max} and z_{\max} can be in excess of 50%. In our sample, one star, W7547, may have such large errors in its orbital parameters.

It should be noted that nearly all of the halo stars have chaotic orbits penetrating the inner 1 kpc of the Galaxy where "scattering" by the bulge generally produces chaos (Schuster & Allen 1997). As shown by Schuster & Allen this introduces considerable noise in the relations between stellar birthplaces and R_{\max} or z_{\max} .

6. Discussion

6.1. The α -elements O, Mg, Si, Ca and Ti

The abundances of the α -elements relative to iron are plotted vs. [Fe/H] in Fig. 4 with different symbols for disk and halo stars. The disk stars follow about the same trend as seen in Edvardsson et al. (1993): i.e. a constant α/Fe ratio for [Fe/H] < -0.6 and then a drop to solar ratios for higher metallicities. The dispersions around the plateau values are about the same as the errors estimated in Table 4. Among the halo stars a small group, plotted with filled circles, follows the trend of the disk stars, except that one of them, HD 106038, is very rich in Si. Another group of halo stars, plotted with open circles, deviate, however, systematically from the disk stars by lying below the disk-plateau in all five diagrams. In the metallicity range, $-1.0 < [\text{Fe}/\text{H}] < -0.7$ the deviation is particularly significant being 3 to 5 times the estimated errors. It should be emphasized that these deviations cannot be explained by systematic errors in the abundance ratios as a function of T_{eff} or $\log g$, because the deviating halo stars

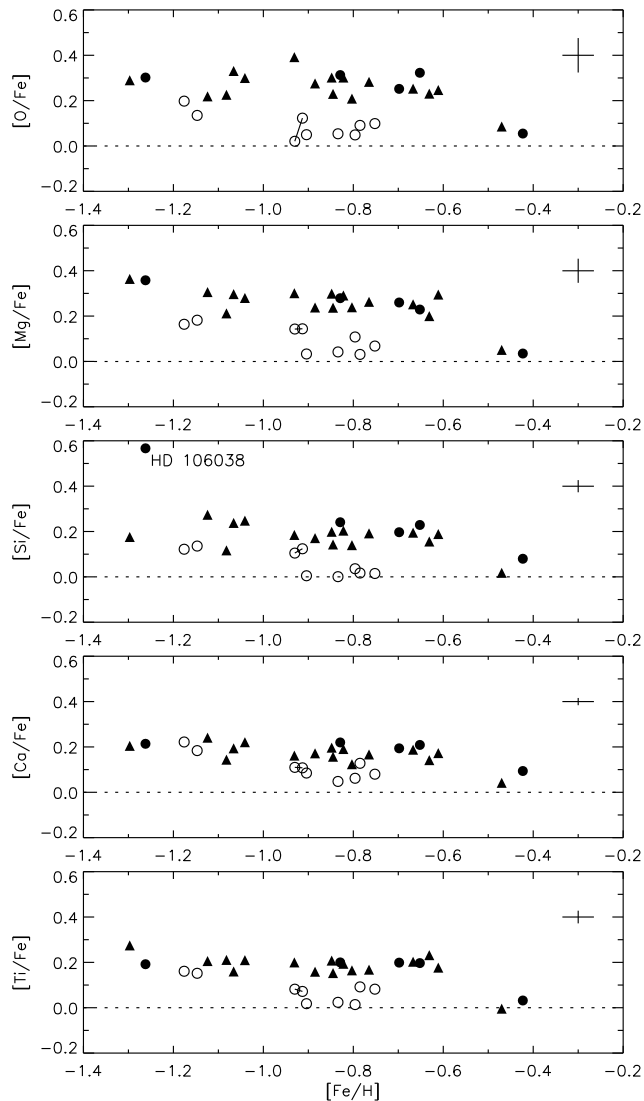


Fig. 4. Abundances of the α -elements relative to iron vs. $[\text{Fe}/\text{H}]$. Disk stars are plotted with filled triangles, and halo stars that follow the trend of the disk stars are shown with filled circles. Deviating halo stars are plotted with open circles. The two components of HD 113083 are connected with a straight line. Errors bars corresponding to the precision of the differential abundance ratios are shown to the right in each figure

have about the same distribution of these two parameters as the disk stars.

A possible interpretation of Fig. 4 is that the α -deficient halo stars have been formed in a region of the Galaxy, where the chemical evolution has proceeded more slowly than in the disk, i.e. with a relatively low star formation rate. This would mean that the delayed iron contribution from Type Ia SNe occurred at a lower metallicity in this region than in the disk. Even within the disk there may be differences in the rate of chemical evolution. Small differences in α/Fe were found by Edvardsson et al. (1993) for disk stars in the metallicity range $-0.6 < [\text{Fe}/\text{H}] < -0.4$. These differences are correlated with

the kinematics of the stars in a way that seems to indicate a faster chemical evolution in the inner parts of the Galactic disk than in the outer parts. The differences in α/Fe seen in Fig. 4 occur in a lower metallicity range ($-1.0 < [\text{Fe}/\text{H}] < -0.7$) than the corresponding differences in the disk, suggesting that the chemical evolution in the halo region has been even slower than in the outer parts of the disk.

In other words: The α -deficient halo stars have been formed in a region of the halo where the interstellar gas was enriched with the nucleosynthesis products of type Ia SNe (i.e. mainly iron) at an unusually low metallicity. The anomaly of the stars is therefore mainly due to their high content of Fe for a given α -element content, and it may therefore be more appropriate to name the stars as “iron rich”. In this connection it is interesting that while type Ia SNe do not produce O and Mg they are thought to contribute some Si, Ca and Ti. According to the detailed nucleosynthesis calculations by Tsujimoto et al. (1995) the relative contribution of SNe Ia to the abundances of Si, Ca and Fe in the Sun is 0.17, 0.25 and 0.57, respectively. This means that the amplitude of the variations of $[\text{Si}/\text{Fe}]$ and $[\text{Ca}/\text{Fe}]$ is expected to be 30–45% less than the amplitude of the $[\text{O}/\text{Fe}]$ and $[\text{Mg}/\text{Fe}]$ variations in good agreement with Fig. 4. Ti was not included in the estimates of Tsujimoto et al. due to uncertainties in the calculation of SNe II yields, but as seen from Fig. 4, Ti seems to follow Ca with perhaps a slightly larger amplitude.

As an interesting alternative, the α -deficient halo stars might have been accreted from dwarf galaxies. Several chemical evolution models for dwarf galaxies, e.g. the Magellanic Clouds, predict a low (i.e. solar) α/Fe ratio for metallicities around $[\text{Fe}/\text{H}] = -1.0$ as a consequence of an early star formation burst followed by a long dormant period (Gilmore & Wyse 1991, Tsujimoto et al. 1995). Even lower α/Fe ratios can be obtained if an enriched galactic wind is added (Pilyugin 1996).

6.2. Na, Cr, Ni, Y and Ba

The abundances of the remaining elements are shown in Fig. 5 with the same symbols as used in Fig. 4. As seen, the ratios of Cr, Y and Ba relative to Fe are close to solar except for the high abundance of the *s*-process elements in HD 106038. The scatter in $[\text{Cr}/\text{Fe}]$ for the disk stars is ± 0.018 dex, i.e. as small as the error estimate in Table 4. The α -deficient halo stars appear slightly underabundant in Cr ($\langle [\text{Cr}/\text{Fe}] \rangle = -0.039$). This agrees with the explanation of the α -deficient stars discussed in the previous section. According to Tsujimoto et al. (1995) the Cr/Fe ratio from the nucleosynthesis contribution of SNe Ia is slightly smaller than that from SNe II.

The most interesting result seen in Fig. 5 is the large Na/Fe deficiencies of the α/Fe -deficient stars, and their smaller but very significant deficiencies in Ni/Fe. These anomalies can be directly seen from the spectra of the stars. Fig. 6 shows a comparison between a disk star and a Na-Ni deficient halo star. Although the two stars have nearly the same T_{eff} and have the same strength of the Fe I lines, the Na I lines differ by about a factor of two in the equivalent widths.

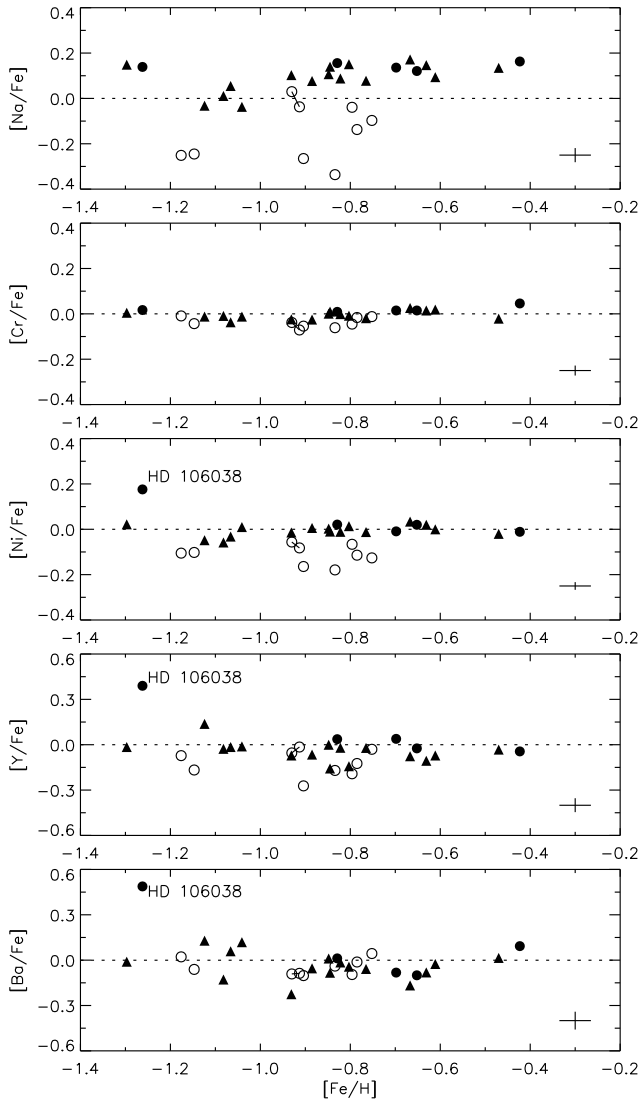


Fig. 5. Abundances of the Na, Cr, Ni, Y and Ba relative to iron vs. [Fe/H]. The symbols used are the same as in Fig. 4

Sodium is expected to be made during carbon and neon burning in massive stars and is expelled by type II SNe together with O and Mg. SNe Ia make only very small amounts of Na (Nomoto et al. 1984, Tsujimoto et al. 1995). Hence, one would expect Na to be closely related to the abundance of Mg and O. The amount of Na made is, however, controlled by the neutron excess, which depends on the initial heavy element abundance in the star (Arnett 1971). Altogether, one expects a relation $[Na/Mg] = a [Mg/H] + \text{const.}$, where $a > 0$. Fig. 7 shows that this is indeed the case. The best straight-line fit to the data is

$$[Na/Mg] = 0.55 [Mg/H] + 0.18 \pm 0.05 \pm 0.03, \quad (2)$$

with a reduced chi-square of 1.7 if the error estimates in Table 4 are adopted. In particular, it is noted that the α -deficient stars

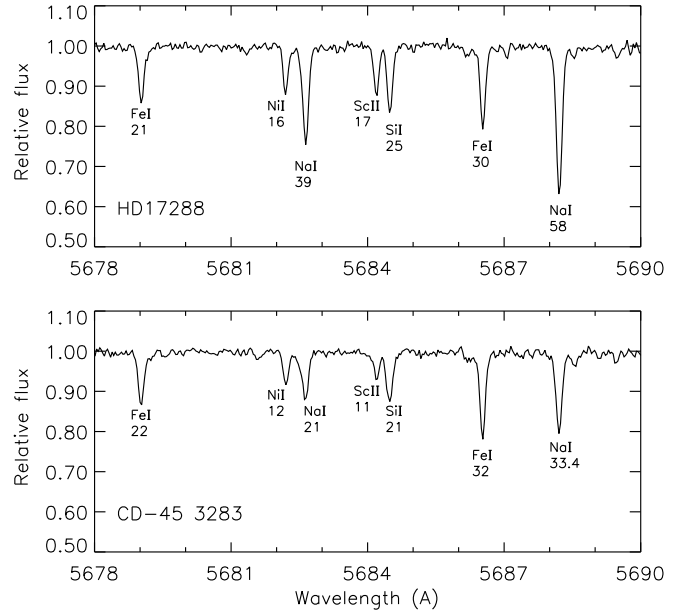


Fig. 6. A comparison of the spectra of HD 17288 and CD-45 3283 in the 5678-5690 Å region. Each line is designated with its equivalent width in mÅ. The two stars have similar values of T_{eff} , $\log g$ and [Fe/H], (5714 K, 4.44, -0.88) and (5672 K, 4.57, -0.83), respectively, and the Fe I lines have nearly the same equivalent widths. The Na lines are, however, much weaker in CD-45 3283 than in HD 17288. Differences in the strengths of the Si and Ni lines are also seen

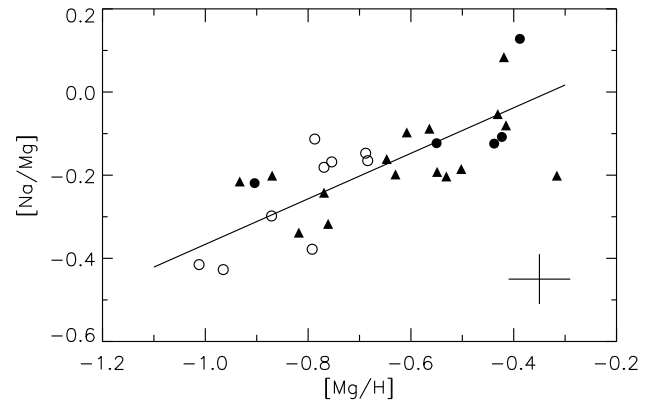


Fig. 7. [Na/Mg] vs. [Mg/H] with the same symbols as used in Fig. 4.

do not have an anomalous position with respect to the disk stars in Fig. 7.

The Ni/Fe deficiency of the α -deficient halo stars is more puzzling. According to Tsujimoto et al. (1995) the contribution of SNe Ia relative to SNe II is higher for Ni than for Fe. Hence, one might have expected a higher than solar Ni/Fe if the α -deficient stars were formed in a halo region that was contaminated by the nucleosynthesis products of SNe Ia. Furthermore, there is a surprisingly tight correlation between Ni/Fe and Na/Fe as seen from Fig. 8. Excluding the special Ni-rich star

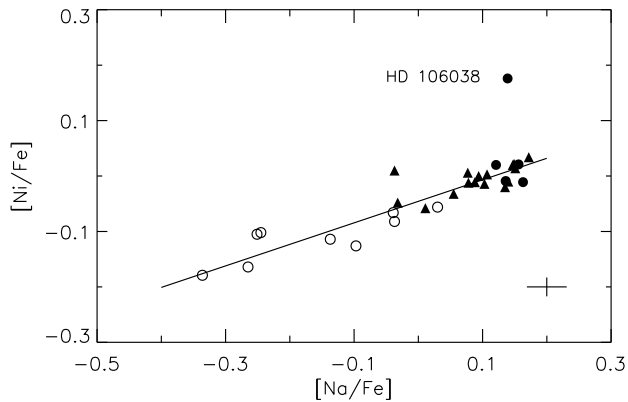


Fig. 8. $[\text{Ni}/\text{Fe}]$ vs. $[\text{Na}/\text{Fe}]$ with the same symbols as in Fig.4

HD 106038 the best straight-line fit to the data is

$$[\text{Ni}/\text{Fe}] = 0.388 [\text{Na}/\text{Fe}] - 0.045 \quad (3)$$

$$\pm .020 \quad \pm .003,$$

with a reduced chi-square of 1.3 if the error estimates in Table 4 are adopted. Thus, it seems that Ni is more closely related to the α -elements and Na than to iron.

Adopting the yields of Type II SNe given by Tsujimoto et al. (1995) it can be investigated if variations in the Initial Mass Function (IMF) can explain the abundance anomalies of the α -deficient halo stars. Integrating the production of the various elements from 10 to 50 solar masses and assuming a Salpeter IMF, $dN/dM \propto M^{-(1+x)}$, it is found that a variation of x from 1.35 to about 2.35 can reproduce the variations seen in Fig. 4, although the predicted change in $[\text{Ca}/\text{Fe}]$ is somewhat too high. There is however no change in $[\text{Ni}/\text{Fe}]$. $[\text{Ni}/\text{Fe}]$ is constant within ± 0.01 for a large range in x .

The puzzlingly low values of $[\text{Ni}/\text{Fe}]$ in the α -deficient halo stars may have something to do with the type of SNe Ia's that produced the iron peak elements. As discussed by Ruiz-Lapuente & Filippenko (1993) on the basis of nucleosynthesis calculations by Nomoto et al. (1984) and Thielemann et al. (1986) the expected $[\text{Ni}/\text{Fe}]$ ratio is quite sensitive to the assumed model. Their W7 model produces a $[\text{Ni}/\text{Fe}]$ ratio that is about a factor of 2 higher than the C6 model. In the W7 model material is accreted onto a white dwarf which has cooled down somewhat, whereas in the C6 model material is accreted onto the C+O core of an AGB star. However, according to Tsujimoto et al. (1995), the Type Ia supernova explosions produce almost no Na and so cannot be used to explain the $[\text{Ni}/\text{Fe}]$ vs. $[\text{Na}/\text{Fe}]$ correlation seen in Fig. 8.

Nucleosynthesis calculations show that the yields of both the dominant Ni isotope (^{58}Ni) and of Na depend upon the neutron excess within the stellar interior (Thielemann et al. 1990). It is proposed here that the heavy element abundances, including the α -elements, control the neutron excesses in SNe II, and that the correlation of Fig. 8 is produced by the SNe II after the first SNe I have begun to modify the α/Fe ratio. This would explain

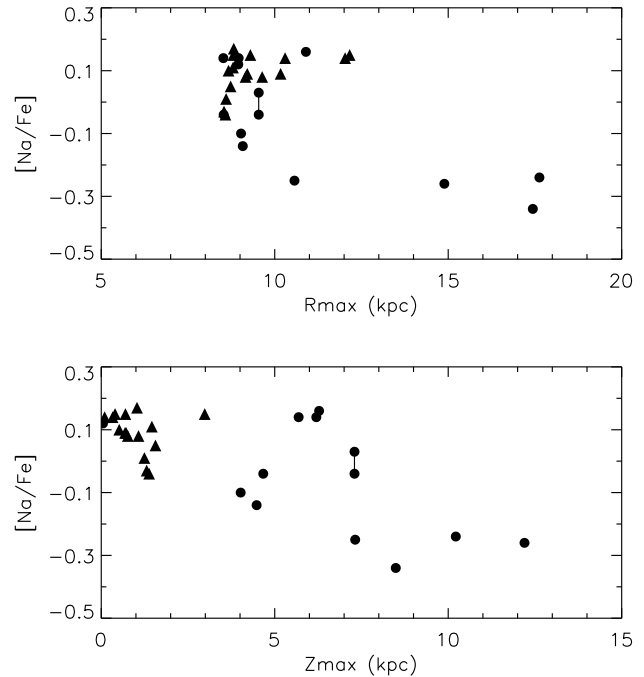


Fig. 9. $[\text{Na}/\text{Fe}]$ vs. the orbital parameters R_{max} and z_{max} . Disk stars are plotted with filled triangles and halo stars with filled circles. Note that the star, W7547, with very large and uncertain values of R_{max} and z_{max} falls outside the intervals shown for these parameters

why Ni (and Na) correlate more closely to the α -elements than to iron.

6.3. Correlations with orbital parameters

Fig. 9 shows the relations between $[\text{Na}/\text{Fe}]$ and R_{max} and z_{max} , respectively. Since $[\text{Na}/\text{Fe}]$ is well correlated with $[\alpha/\text{Fe}]$ and $[\text{Ni}/\text{Fe}]$, a similar dependence on R_{max} and z_{max} is found for these abundance ratios. There appears to be a tendency for stars with large values of R_{max} and z_{max} to have relatively low values of $[\alpha/\text{Fe}]$, $[\text{Na}/\text{Fe}]$ and $[\text{Ni}/\text{Fe}]$. Clearly, a larger sample of stars is needed before any strong conclusions can be made, and, as discussed in Sect. 5.2, R_{max} and z_{max} may not be entirely accurate indicators of stellar birthplaces. Still, Fig. 9 could be taken as support for the suggestion made in Sect. 6.1 that the α -deficient stars have been accreted from dwarf galaxies, or, at least, from low-density regions of the outer halo where the chemical evolution proceeded more slowly than in the inner halo as predicted from the models of galaxy formation by Matteucci & François (1992) and discussed in some detail by Matteucci (1992). The dichotomy in $[\alpha/\text{Fe}]$ may therefore be related to the duality of the Galactic halo discussed by Zinn (1993) and by Marquez & Schuster (1994): The α -poor halo stars belong to the outer accreted halo, whereas the α -rich stars belong to the inner, proto-disk halo.

In a recent paper on sodium abundances in 60 metal-poor subgiants and giants, Pilachowski et al. (1996) find a wide scatter in $[\text{Na}/\text{Fe}]$ from -0.6 to nearly $+0.3$, and suggest “that the

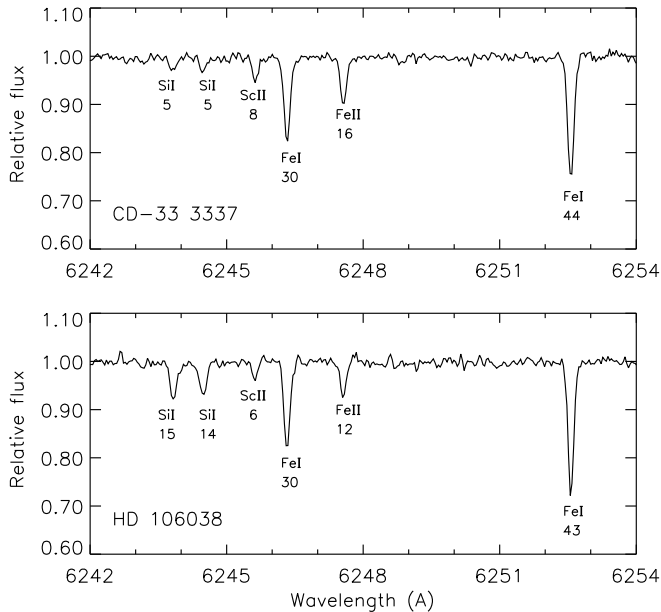


Fig. 10. A comparison of the spectra of CD-33 3337 and HD 106038 in the 6242-6254 Å region. Each line is designated with its equivalent width in mÅ. The two stars have similar values of T_{eff} , and $[\text{Fe}/\text{H}]$, (6097 K, -1.30) and (6046 K, -1.26), respectively, but the gravities are different (4.09 and 4.44). The Fe I lines have nearly the same equivalent widths, but the Si I lines are a factor of 3 stronger in HD 106038 than in CD-33 3337. The small differences in the strengths of the ionized lines are due to the difference in $\log g$

production of Na in the Galactic halo was highly localized in space and perhaps in time”. They do not study possible correlations between $[\text{Na}/\text{Fe}]$ and abundance ratios like $[\text{Mg}/\text{Fe}]$ and $[\text{Ni}/\text{Fe}]$ or between $[\text{Na}/\text{Fe}]$ and stellar orbital parameters. In view of the results in the present paper such correlations should be looked for.

6.4. HD 106038

As seen from Table 3 and Figs. 4 and 5, HD 106038 is very rich in Si, Ni, Y, and Ba relative to Fe, although it has atmospheric parameters, $T_{\text{eff}} = 6050$ K, $\log g = 4.5$ and $[\text{Fe}/\text{H}] = -1.3$, typical of a main sequence star. The overabundance of Si is particularly high and can be directly seen in its spectrum, when the star is compared with other stars with similar atmospheric parameters; Fig. 10. Furthermore, the Li I 6707.8 Å line is unusually strong with an equivalent width of $W = 61$ mÅ. According to a preliminary analysis (Fredsgaard 1996) $\log \epsilon(\text{Li}) = 2.6$, which places HD 106038 well above the “Spite plateau”.

The high abundances of Y and Ba might suggest that HD 106038 is of the same type as the CH subgiants (Luck and Bond 1991), for which the overabundance of the *s*-process elements is explained as a result of a mass transfer from an AGB star in a binary system. Tomkin et al. (1989) have found a main sequence F star of the same type. There is, however, no sign of a component in the radial velocity measurements. According to Carney et al. (1994), $V_r = 99 \pm 0.4$ km s $^{-1}$ for 6 ob-

servations. Furthermore, the CH subgiants do not have large overabundances of Li, Si and Ni.

7. Conclusions

High resolution ($R = 60\,000$), high signal-to-noise spectra ($S/N \simeq 150$) have been obtained with the ESO NTT EMMI spectrograph equipped with an R4 echelle grating. Equivalent widths of weak lines are used to determine very precise values of T_{eff} , $\log g$ and abundances for 13 halo and 16 disk stars, which overlap in metallicity in the range $-1.3 \lesssim [\text{Fe}/\text{H}] \lesssim -0.5$. The stars are on or near the main sequence and are confined to a rather small range in effective temperature, $5400 \lesssim T_{\text{eff}} \lesssim 6500$ K. The precision of the relative abundance ratios range from 0.02 dex for $[\text{Ca}/\text{Fe}]$ and $[\text{Ni}/\text{Fe}]$ to 0.07 dex for $[\text{O}/\text{Fe}]$.

The disk stars in the metallicity range $-1.3 \lesssim [\text{Fe}/\text{H}] \lesssim -0.6$ are found to have nearly constant abundance ratios α/Fe , Na/Fe, Cr/Fe, Ni/Fe, Y/Fe and Ba/Fe. The dispersions are as small as the estimated precision of the determinations. The halo stars, however, show a very significant cosmic spread in these ratios with a tendency to fall into two separate groups. Five stars have nearly the same abundance ratios as the disk stars, except for HD 106038, which is found to be peculiarly rich in Si, Ni, Y and Ba. The other 8 halo stars have significantly lower ratios of $[\text{O}/\text{Fe}]$, $[\text{Na}/\text{Fe}]$, $[\text{Mg}/\text{Fe}]$, $[\text{Si}/\text{Fe}]$, $[\text{Ca}/\text{Fe}]$, $[\text{Ti}/\text{Fe}]$ and $[\text{Ni}/\text{Fe}]$ than the disk stars. Furthermore, the majority of these halo stars have larger values of the orbital parameters R_{max} and z_{max} . This may suggest that the α -deficient stars belong to the outer accreted halo, whereas the α -rich stars belong to the inner proto-disk halo. The α -deficiency at $[\text{Fe}/\text{H}] \simeq -1.0$ can then be explained as a result of the special chemical evolution history of dwarf galaxies characterized by an early burst of star formation followed by a dormant period with SNIa enrichment. Clearly, these suggestions should be tested for a much larger sample of stars. In any case the data show that the chemical evolution of the Galaxy is more inhomogeneous around $[\text{Fe}/\text{H}] \simeq -1$ than assumed in many models.

$[\text{Na}/\text{Mg}]$ is well correlated with $[\text{Mg}/\text{H}]$ ($[\text{Na}/\text{Mg}] \simeq 0.5[\text{Mg}/\text{H}] + \text{const.}$), as expected if sodium is made during carbon and neon burning in massive stars with the neutron excess controlled by their initial heavy element abundance. The Ni/Fe deficiencies in the 8 halo stars may have been caused in part by the SNe Ia, but the tight relation between $[\text{Ni}/\text{Fe}]$ and $[\text{Na}/\text{Fe}]$ shown in Fig. 8 is probably due to type II SNe yields depending on neutron excess. Finally, the peculiar composition of HD 106038 remains a mystery, in particular because the radial velocity measurements show no sign of a component.

Acknowledgements. Bengt Edvardsson is thanked for constructing the net of model atmospheres used for the abundance analysis of the equivalent widths, and Christine Allen for computing stellar orbits. J. Andersen, B. Edvardsson, B. Gustafsson and B. Pagel are thanked for very useful comments on a first version of the paper. This work was partially supported by grants from CONACyT, Nos. D111-903865 and 1219-E9203, and DGAPA project No. IN101495. Use was made of the SIMBAD database operated at CDS, Strasbourg, France.

Appendix A

A number of tables containing more detailed data for the program stars are available in electronic form from CDS by anonymous ftp to 130.79.128.5. Here a brief description of these tables is given.

Table A1 lists the Strömrgren photometry together with color excesses, $E(b-y)$, photometric metallicities, $[Fe/H]$, calculated from the calibrations of Schuster & Nissen (1989), and absolute magnitudes, M_V , and distances derived with the equations of Nissen & Schuster (1991).

Table A2 contains coordinates, proper motions and radial velocities for the program stars.

Table A3 gives a list of the 209 spectral lines, which were analyzed, arranged element by element. The table contains the wavelength, the excitation potential of the lower level corresponding to the line, the gf -value, the enhancement factor of the classical van der Waals damping constant, the statistical weight of the upper level, and the equivalent widths measured for the two “standard” stars, HD 22879 and HD 76932.

Table A4 contains the measured equivalent widths for all the program stars.

Table A5 gives abundance ratios and kinematical as well as orbital parameters for the program stars.

References

- Allen C., Martos M.A. 1986, *Rev. Mex. Astron. Astrofis.* 13, 137
- Allen C., Santillán A. 1991, *Rev. Mex. Astron. Astrofis.* 22, 255
- Allen C., Schuster W.J., Poveda A. 1991, *A&A* 244, 280
- Arnett W.D. 1971, *ApJ* 166, 153
- Asplund M., Gustafsson B., Kiselman D., Eriksson K. 1997, *A&A* 318, 521
- Barbier-Brossat M., Petit M. 1986, *A&AS* 65, 59
- Beers T.C., Sommer-Larsen J. 1995, *ApJS*, 96, 175
- Bergbusch P.A., VandenBerg D.A. 1992, *ApJS* 81, 163
- Blitz L., Teuben P. (eds.) 1996, *IAU Symp.* 169, “Unsolved Problems of the Milky Way”, Kluwer, Dordrecht
- Carney B.W., Latham D.W., Laird J.B., Aguilar L.A. 1994, *AJ* 107, 2240
- Carney B.W., Laird J.B., Latham D.W., Aguilar L.A. 1996, *AJ* 112, 668
- Dekker H., D’Odorico S., Fontana A. 1994, *The ESO Messenger* No. 76, 16
- Eggen O.J., Lynden-Bell D., Sandage A.R. 1962, *ApJ* 136, 748
- Edvardsson B., Andersen J., Gustafsson B., Lambert D.L., Nissen P.E., Tomkin J. 1993, *A&A* 275, 101
- Fouts G., Sandage A. 1986, *AJ* 91, 1189
- Fredsgaard B. 1996, Masters Thesis, Århus University
- Gilmore G., Wyse R.F.G. 1991, *ApJ* 367, L55
- Gustafsson B., Bell R.A., Eriksson K., Nordlund Å. 1975, *A&A* 42, 407
- Heney L., Vardya M.S., Bodenheimer P. 1965, *ApJ* 142, 841
- Johnson D.R.H., Soderblom D.R. 1987, *AJ* 93, 864
- Latham D.W., Mazeh T., Stefanik R.P. et al. 1992, *AJ* 104, 774
- Lindgren H. 1994, Ph. D. Thesis, Lund University
- Lindgren H., Ardeberg A., Zuiderwijk E. 1989, *A&A* 218, 111
- Luck R.E., Bond H.E. 1991, *ApJS* 77, 515
- Marquez A., Schuster W.J. 1994, *A&AS* 108, 341
- Matteucci F. 1992, in “Morphological and Physical Classification of Galaxies”, eds. G. Longo et al., Kluwer, Dordrecht, p. 245
- Matteucci F. 1996, *IAU Symp.* 169, “Unsolved Problems of the Milky Way”, eds. L. Blitz and P. Teuben, Kluwer, Dordrecht, p.367
- Matteucci F., François P. 1992, *A&A* 262, L1
- Mihalas D., Binney J. 1981, *Galactic Astronomy*, W.H. Freeman and Company, New York
- Nissen P.E., Schuster W.J. 1991, *A&A* 251, 457
- Nissen P.E., Twarog B.A., Crawford D.L. 1987, *AJ* 93, 634
- Nomoto K., Thielemann F.-K., Yokoi K. 1984, *ApJ* 286, 644
- Norris J.E. 1996, in “Formation of the Galactic halo, inside and out”, eds. H.L. Morrison and A. Sarajedin, San Francisco, ASP (in press)
- Pagal B.E.J., Tautvaišienė G. 1995, *MNRAS* 276, 505
- Pilachowski C.A., Sneden C., Kraft R.P. 1996, *AJ* 111, 1689
- Pilyugin L.S. 1996, *A&A* 310, 751
- Ruiz-Lapuente P., Filippenko A.V. 1993, in “Origin and Evolution of the Elements”, eds. N. Prantzos, E. Vangioni-Flam and M. Cassé, Cambridge Univ. Press, p.318
- Schuster W.J., Allen C. 1997, *A&A*, 319, 796
- Schuster W.J., Nissen P.E. 1988, *A&AS* 73, 225
- Schuster W.J., Nissen P.E. 1989, *A&A* 221, 65
- Schuster, W.J., Parrao, L., Contreras Martínez, M.E. 1993, *A&AS*, 97, 951
- Thielemann, F.-K., Nomoto K., Yokoi K. 1986, *A&A* 158, 17
- Thielemann, F.-K., Hashimoto M., Nomoto K. 1990, *ApJ* 349, 222
- Tomkin J., Lambert D.L., Edvardsson B., Gustafsson B., Nissen P.E. 1989, *A&A* 219, L15
- Tsujimoto T., Nomoto K., Yoshii Y., Hashimoto M., Yanagida S., Thielemann F.-K. 1995, *MNRAS* 277, 945
- Turon C., Crézé M., Egret D., et al. 1992, *The Hipparcos Input Catalogue*, European Space Agency Publications Division, Noordwijk, The Netherlands
- Wyse R.F.G., Gilmore G. 1993, *ASP Conf. Ser.* 48, “The Globular Cluster-Galaxy Connection”, eds. G.H. Smith and J.P. Brodie, p.727
- Zinn R. 1993, *ASP Conf. Ser.* 48, “The Globular Cluster-Galaxy Connection”, eds. G.H. Smith and J.P. Brodie, p.38